

Resolution Measurement for Synthetic Aperture Sonar

Jeremy Dillon
Kraken Robotic Systems Inc.
Mount Pearl, NL, Canada
jdillon@krakenrobotics.com

Richard Charron
Kraken Robotic Systems Inc.
Mount Pearl, NL, Canada
rcharron@krakenrobotics.com

Abstract—The theoretical resolution of a Synthetic Aperture Sonar (SAS) is determined by the -3 dB beamwidth of its two-way element beampattern. In practice, resolution may be degraded by unknown factors such as imperfect estimation of the platform trajectory, seabed topography, and refractive effects due to the sound velocity profile. Methods to automatically assess the resolution practically achieved are useful for quality control and for adaptive mission planning. We show how the range-azimuth SAS point spread function can be estimated using only the autocorrelation properties of seabed reverberation. Experimental results are presented for AquaPix[®], a wideband 300 kHz interferometric SAS.

Index Terms—synthetic aperture sonar, resolution, autocorrelation, reverberation, point spread function

I. INTRODUCTION

The resolution of a sonar image determines the length scale of the smallest objects that can reliably be detected on the seabed or in the water column. Minimizing this resolution length scale is desirable for applications such as seabed surveying for oil and gas extraction, benthic habitat mapping for fisheries research, and mine detection and classification for underwater defence. When a sonar is used for Mine Countermeasures (MCM), the resolution affects the achievable detection probability and false alarm rate, with 5 cm resolution quoted as a typical value for adequate target classification performance [1].

Let x and y denote the along track and across track directions (also known as across range and along range, or azimuth and range). For a sidelooking geometry, the sonar transmits acoustic pulses in the y direction while travelling in the x direction. Across track resolution is typically achieved by transmitting a broadband signal, such as a linear frequency modulated chirp, and applying a matched filter to the received echoes, resulting in an across track resolution δ_y of [2]

$$\delta_y = \frac{C}{2B} \quad (1)$$

where $C \approx 1500 \text{ m s}^{-1}$ is the speed of sound in water and B is the bandwidth of the transmitted pulse. Thus, a bandwidth of approximately 15 kHz is required to achieve 5 cm across track resolution, which is easily achievable using commercial off-the-shelf (COTS) transducer and electronics technology.

For a conventional sidescan sonar, the angular width of the transmitted beam is determined by the along track length L

of the transmitting element (or array of elements) relative to the acoustic wavelength λ . The along track resolution is approximately given by

$$\delta_x = \frac{R\lambda}{L}, \quad (2)$$

which increases linearly with range R to the target. For a stand-off range of 100 m, an array length of 2000λ is required to achieve 5 cm along track resolution. The array length is typically constrained by the available space on an underwater vehicle or towed body, and by the distortion that results from subjecting a long array to pressure loads that vary with depth. For example, if the array length is limited to 2 m, a wavelength of 1 mm corresponds to an operating frequency of 1.5 MHz, which causes sound waves to be severely attenuated by absorption in seawater.

The trade-off between range, array length, and wavelength in (2) is circumvented in SAS image formation by utilizing the forward motion of the sonar platform to synthesize a long array from multiple pings. The result is an along track resolution that is proportional to the effective transmitter length and independent of both range and frequency. Therefore, 5 cm resolution can be achieved with a wide transmission beam (e.g. by choosing a sufficiently *short* transmitter) if the image from the synthetic array can be properly focused.

In practice, the theoretical resolution may be degraded by factors such as vehicle stability, environmental conditions, multi-path propagation, ambient noise, seabed characteristics, in addition to the design of the sonar array and electronics [3]. Thus, in the literature one may find statements such as “with other standard COTS SAS systems ... the effective gain ... is not always the gain that is claimed by the manufacturer” [4]. When a manufacturer claims a theoretical resolution of “ 2×2 cm” and a practical resolution of “ $< 5 \times 5$ cm” [5], it is understandable that the end user may be confused as to how these values are defined and measured, and what may be expected in a given environment. Also, there is a tendency to show images of shipwrecks such as Figure 1 for promotional purposes. While such images are visually appealing, the length scale of a shipwreck does not facilitate evaluation of resolution at the centimetre level.

The resolution of an imaging system is defined in terms of the point spread function, i.e. the response to an idealized

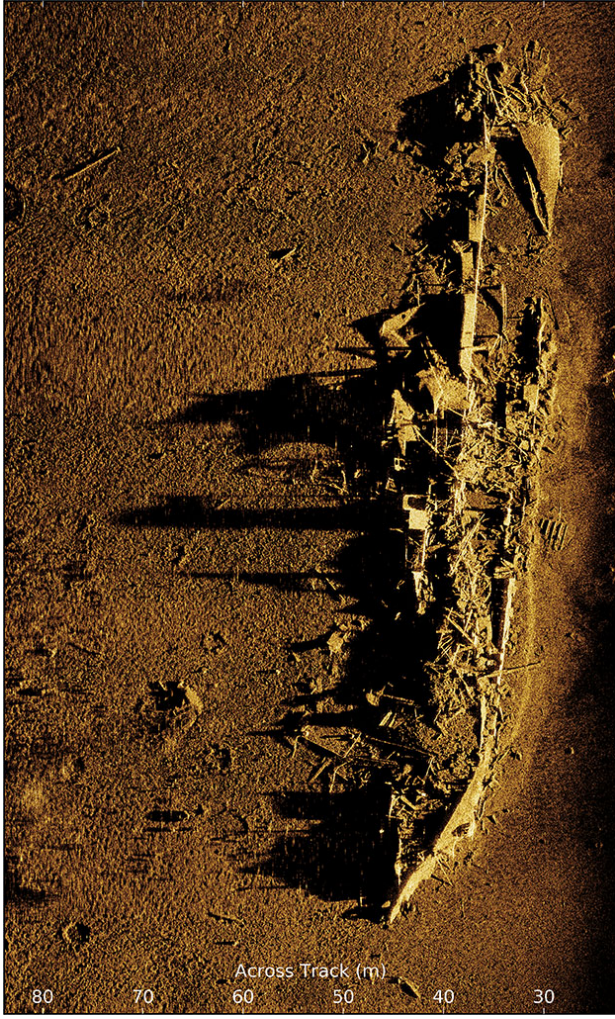


Fig. 1. AquaPix SAS image of the SS Ferrando shipwreck provided courtesy of ECA Robotics.

point target, or in practice, an object significantly smaller than the resolution length scale. Given that typical SAS resolutions are on the order of centimetres, it is impractical to deploy sufficiently small point targets in a realistic operating environment.

In this paper, we present a simple method for estimating the resolution of a SAS from only the autocorrelation properties of seabed reverberation. Unlike other methods such as [6], it is not necessary to assume a point-like response from discrete isolated scatterers. Instead, the proposed method only requires the distribution of scatterers to be isotropic, or similarly distributed in the along track and across track directions. The method can be applied to any SAS image thereby facilitating a comparison of systems from various manufacturers using a common criterion. Additionally, the method is sufficiently simple to implement that it raises the interesting possibility of estimating resolution “on-the-fly” while adapting the mission plan of an Autonomous Underwater Vehicle (AUV) to achieve a desired probability of detection during MCM operations.

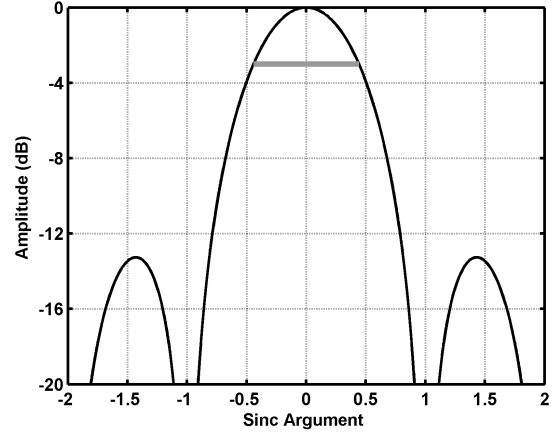


Fig. 2. Amplitude response of the sinc function in (4). The -3 dB width is indicated by the grey line.

II. THEORY

A. Resolution criterion

To motivate the precise definition of resolution, we first consider a highly simplified model of synthetic aperture image formation. The signal $\exp(i\omega t)$ is transmitted from each element location and echoes are received from a point target located at range and bearing (R, θ) in the far field of the array. Ignoring range dependent scale factors, the coherent sum $z(t)$ of the received echoes is given by [2]

$$\begin{aligned} z(t) &= \sum_{n=-M}^M \exp \left\{ i\omega \left[t - \frac{2}{c}(R - nd \sin \theta) \right] \right\} \\ &= e^{i(\omega t - 2kR)} \frac{\sin[(2M+1)kd \sin \theta]}{\sin(kd \sin \theta)} \end{aligned} \quad (3)$$

where d is the spacing between receiver elements and k is the wavenumber ω/c . If a small angle approximation is invoked for the denominator of (3), the normalized amplitude A of $z(t)$ simplifies to

$$A = \left| \text{sinc}(2L_{\text{SAS}} \sin \theta / \lambda) \right| \quad (4)$$

where L_{SAS} is the length $(2M+1)d$ of the synthetic aperture and “sinc” is the normalized sinc function $\sin(\pi x)/\pi x$.

There are several commonly accepted definitions for the resolution of an imaging system. For example, the Rayleigh criterion of resolution is defined as the distance between locations of the maximum and the first null of the amplitude pattern [7]. The first null in (4) occurs when

$$\sin \theta = \frac{\lambda}{2L_{\text{SAS}}}, \quad (5)$$

resulting in an along track resolution

$$\delta_x = R \sin \theta = \frac{R\lambda}{2L_{\text{SAS}}}. \quad (6)$$

The length of the synthetic aperture is limited by the beamwidth of the transmitter and receiver elements. The maximum aperture length is typically taken to be

$$L_{\text{SAS}} = \frac{R\lambda}{L_t} \quad (7)$$

where λ/L_t represents the beamwidth of the two-way element beampattern (L_t is the equivalent length of the transmitter). Combining (6) and (7), the SAS resolution is

$$\delta_x = \frac{L_t}{2}, \quad (8)$$

which is independent of both range and frequency.

The impulse response of a SAS may deviate from the sinc pattern (3) and nulls may be non-existent or difficult to locate when aperture shading is applied to suppress sidelobes. A more robust definition of resolution is obtained by specifying the half-power beamwidth of the impulse response [8]. As shown in Figure 2, this definition is similar to the Rayleigh criterion because the -3 dB width of a sinc function is equal 0.886 times the distance to the first null (located at an abscissa of 1). Equation (4) is an approximation because it has been assumed that the spatial frequency response in the azimuth direction is flat, with a rectangular window spanning the two-way beamwidth of the transmit-receive system. In practice, the beam pattern is not flat, and furthermore, an along track shading function is applied during SAS processing to suppress sidelobes. The along track resolution based on half-power beamwidth is therefore given by

$$\delta_x = 0.886 \frac{L_t}{2} \gamma_x, \quad (9)$$

where γ_x is a broadening factor that accounts for a reduction in along track bandwidth due to shading. In many cases, the product of factors $0.886 \gamma_x$ is close to unity, resulting in the commonly quoted expression (8) in the literature. Likewise, the more general form of (1) based on half-power beamwidth is given by

$$\delta_y = 0.886 \frac{C}{2B} \gamma_y, \quad (10)$$

where the broadening factors γ_x and γ_y may differ, for example due to application of different shading functions for along track and across track processing. In Section III, along track resolution is evaluated numerically using measured transmit and receive beam patterns for a shaded synthetic aperture.

B. Image formation

By superposition, a complex-valued SAS image is the convolution of its impulse response with the amplitude and phase distribution of scatterers on the seabed. Scatterers may be regarded as a realization of a random process having a prescribed spatial spectral density. In the case of a flat seabed devoid of man-made objects and naturally occurring features such as ripples, rocks, and vegetation, the spectral density is white noise. It follows from the Wiener-Khinchin theorem [9] that the autocorrelation of the complex SAS image is simply the autocorrelation of the impulse response. This can also be

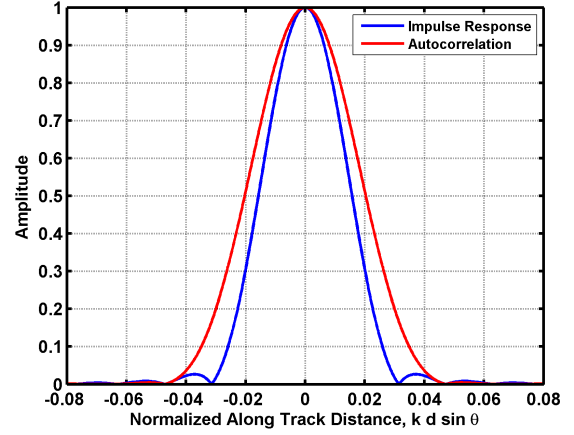


Fig. 3. Impulse response and autocorrelation of the shaded SAS model with $M = 100$. The coherent sum in (3) is weighted with a Hann window.

seen by noting that a point target and white noise have the same autocorrelation function, namely that of a Dirac delta function.

For the simplified model of Section II-A, the along track impulse response is given by (4) and (6),

$$z(x) = \text{sinc}(x/\delta_x), \quad (11)$$

with a corresponding normalized autocorrelation function of

$$\begin{aligned} a(x) &= \frac{\int_{-\infty}^{\infty} z(x+s) \overline{z(s)} ds}{\int_{-\infty}^{\infty} |z(s)|^2 ds} \\ &= \text{sinc}(x/\delta_x). \end{aligned} \quad (12)$$

The autocorrelation function therefore has the same shape as the impulse response. This fact is easily verified by noting that the Fourier transform of a sinc function is a rectangular function.

Typically, some form of aperture shading is applied to suppress sidelobes in the SAS image. The autocorrelation function is therefore broader than the impulse response (i.e. the spatial bandwidth is reduced by shading). For example, when the coherent sum in (3) is weighted with a Hann window, the impulse response and autocorrelation are shown in Figure 3 in terms of the normalized along track distance $kd \sin \theta$ for M equal to 100. In Figure 3, the autocorrelation function is approximately 30% broader than the impulse response. For comparison, the first null of the unshaded amplitude pattern occurs when $kd \sin \theta$ equals $\pi/(2M + 1)$ (approximately 0.016).

The along track focusing of a SAS image can be corrupted, for example, due to unresolved motion errors of the host platform, inaccuracy of the sound velocity measurement, or refractive effects. Defocusing effects can be represented as a phase perturbation $\exp(j\theta(x))$ in the along track raw data prior to SAS beamforming. Defocusing produces an along track smearing in the magnitude of the SAS image (i.e. the real-valued intensity image that is normally displayed with phase

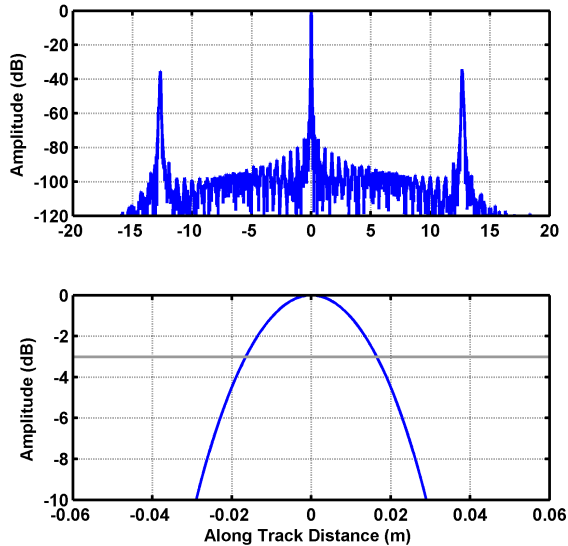


Fig. 4. Simulated along track SAS impulse response at 100 m range using measured AquaPix beam patterns and Hann shading of the synthetic aperture. The grey line in the lower panel indicates the -3 dB level.

information discarded) with a corresponding broadening of the autocorrelation of the intensity image. Somewhat paradoxically, the autocorrelation of the complex image is unchanged compared to the properly focused case because the along track bandwidth is the same in both cases. Defocusing can therefore be detected by comparing the autocorrelation widths for the complex and intensity SAS images. The autocorrelation of the complex image measures the available spatial bandwidth for image formation, which represents a lower bound on the achievable resolution δ_x . The autocorrelation of the intensity image is a biased estimator of the SAS image resolution. The technique presented in this paper uses the *across track* autocorrelation to calibrate and remove the bias from the along track estimate, as described in Section IV-B. This approach therefore avoids the necessity of assuming the presence of distinct point-like targets with dimensions smaller than the SAS resolution. It is only assumed that the distribution of seabed scatterers is isotropic, as is typically the case for a flat featureless seabed.

III. NUMERICAL SIMULATION

The along track resolution of a SAS can be simulated numerically by considering an ideal point target moving past the sonar with a perfectly linear trajectory. At each along track position of the synthetic aperture, the demodulated and matched filtered echo can be represented by a complex number z . For simplicity, it is assumed that the target is centered in the vertical beam of the sonar, the sonar employs a monostatic geometry, and the stop-and-hop approximation is invoked [2]. The relative azimuth angle, or bearing, between the sonar and target is computed for each position. The amplitude of z is obtained via a table lookup from the measured two-way

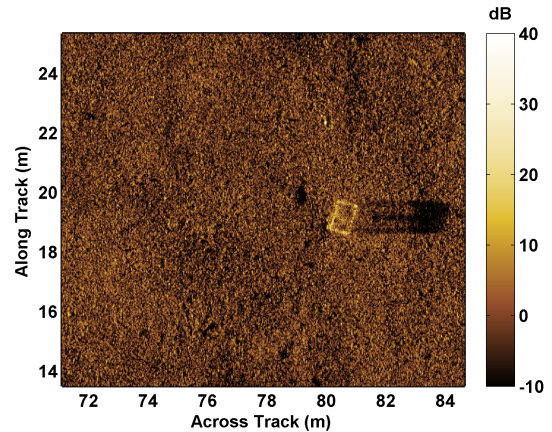


Fig. 5. AquaPix SAS image of a cube-like target and surrounding seabed.

beam pattern of the sonar. Range dependent propagation losses are neglected since the range migration effects on amplitude are negligible for a high frequency SAS. The phase of z is $4\pi R/C$ radians, where R is the one-way propagation distance from the sonar to the target. The impulse response is obtained by applying a SAS image formation algorithm with shading of the along track complex data signal that represents the demodulated target echo. The impulse response is shown in Figure 4. Grating lobes, which are a characteristic of a spatially undersampled SAS, are well suppressed by judicious choice of the transmit and receive beam patterns. In the lower panel, the figure zooms in on the main lobe of the impulse response while showing the -3 dB threshold that defines resolution based on half-power beamwidth. The predicted along track resolution is 3.3 cm, which represents the ideal case where the platform motion is well resolved.

IV. EXPERIMENTAL RESULTS

A. Sea trial

AquaPix is a wideband interferometric SAS featuring a unique dual row design for multipath suppression [10]. The sonar was integrated into an AUV for data collection during sea trials described in [11]. Figure 5 shows an image of a cube-like target and surrounding seabed generated by Kraken's GPU-accelerated backprojection software, which is part of the company's INSIGHT SAS imaging software suite. The pixel spacing is 1.5 cm in the across track direction and 1.67 cm along track. A Hann window was applied in both directions to suppress sidelobes. Visual inspection of the target perimeter in Figure 5 reveals that the along track resolution is slightly broader than the across track resolution, indicating a well focused SAS image. The measured along track resolution is therefore expected to approach the theoretical value presented in Section III. The region selected for autocorrelation analysis is immediately to the left of the target. It can be seen that the selected region is devoid of large scale features such as ripples, rocks, or vegetation.

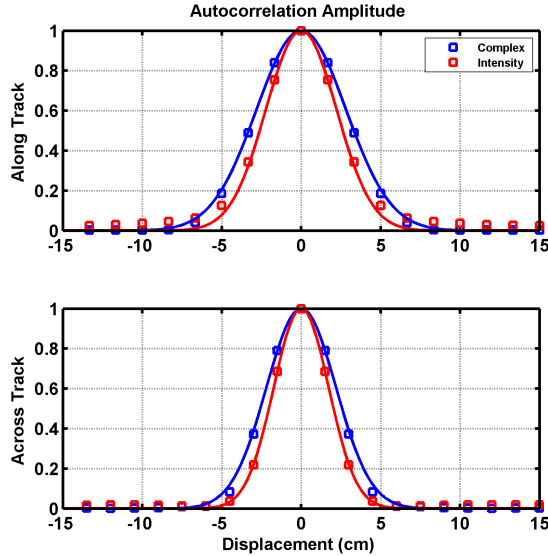


Fig. 6. AquaPix autocorrelation measurements from the SAS image in Figure 5 (squares). Each solid line represents a Gaussian fit to the corresponding measured values.

B. Resolution estimation

The along track and across track autocorrelation functions are plotted in Figure 6 for the complex SAS and intensity SAS images. Measurements are indicated by squares with spacings of 1.67 cm and 1.5 cm for along track and across track directions, respectively. The solid lines are obtained by fitting a Gaussian function to the three highest points of the autocorrelation function (for lags of 0 and ± 1 samples). The autocorrelation functions for a SAS are well described by Gaussian functions due to the Hann windowing and the additional shading provided by the two-way element beampattern.

The width of the Gaussian function is directly related to the autocorrelation amplitude at a lag of one sample. Let a_1 denote the autocorrelation amplitude at a lag x_1 . The width σ_a of the Gaussian autocorrelation function is given by

$$\sigma_a = \frac{x_1}{\sqrt{-2 \ln a_1}} \quad (13)$$

where \ln is the natural logarithm.

A Gaussian autocorrelation function is produced by a Gaussian impulse response with an impulse response width $\sigma_a/\sqrt{2}$. This fact can be verified by noting that the Fourier transform of a Gaussian function is also Gaussian, with spectral width reduced by $\sqrt{2}$ upon exponentiation. Therefore, the corresponding impulse response is given by

$$z(x) = \exp(-x^2/\sigma_a^2) \quad (14)$$

when normalized to have a peak value of 1.

Resolution measurements for each image type and direction are obtained by solving for the distance x_2 at which (14)

TABLE I
MEASURED -3 dB WIDTH

Direction	Image Type	Width (cm)
Along Track	Complex	3.31
Along Track	Intensity	2.61
Across Track	Complex	2.57
Across Track	Intensity	2.03

achieves an amplitude of $1/\sqrt{2}$ corresponding to the -3 dB point. We find that

$$x_2 = \sigma_a \sqrt{\frac{\ln 2}{2}}. \quad (15)$$

The -3 dB width is $2x_2$. Combining (13) and (15), the resolution measurement is

$$\begin{aligned} \delta &= x_1 \sqrt{\frac{\ln 2}{-\ln a_1}} \\ &\approx \frac{0.8326 x_1}{\sqrt{-\ln a_1}}, \end{aligned} \quad (16)$$

where δ represents each of the four combinations of image type and along/across track direction (δ_{xc} , δ_{xi} , δ_{yc} , and δ_{yi} , with subscripts c and i representing complex and intensity images, respectively). For the autocorrelation functions shown in Figure 6, the corresponding resolution measurements are presented in Table I.

In the across track direction, high resolution is obtained via matched filtering. The across track resolution is given by $\delta_y = \delta_{yc}$, or 2.6 cm from Table I. The measured across track resolution is consistent with a transmit pulse bandwidth of 40 kHz and Hann shading applied during matched filtering.

Assuming an isotropic seabed, the ratio δ_{yi}/δ_{yc} provides a measure of the bias inherent in measuring resolution from the intensity image. Along track resolution is estimated as

$$\delta_x = \delta_{xi} \frac{\delta_{yc}}{\delta_{yi}}, \quad (17)$$

which equals 3.3 cm for the values in Table I, in agreement with the theoretical value from Section III.

V. CONCLUSION

In this paper, a simple method has been presented for estimating the resolution of a SAS from only the autocorrelation properties of seabed reverberation. The method allows estimation of resolution at the centimetre-scale without need for deploying reference targets. SAS resolution can therefore be evaluated in realistic operating conditions, for example in the presence of AUV motion errors, ambient noise, a non-uniform sound velocity profile, etc. The resolution criterion is defined in terms of the -3 dB width of the SAS impulse response and it was shown that this definition is consistent with the Rayleigh criterion. The method can be applied to any SAS image, thereby facilitating a comparison of systems from various manufacturers using a common criterion.

Results were presented for AquaPix, a wideband 300 kHz interferometric SAS that was integrated into an AUV for

data collection during sea trials. Shading is applied during SAS image formation to suppress sidelobes. Experimental results indicate that the shaded SAS impulse response is well described by a Gaussian function. In the event that the impulse response is not exactly Gaussian, e.g. as shown for the simplified SAS model with Hann shading in Figure 3, a Gaussian assumption is nevertheless a useful approximation for the purpose of determining the -3 dB width. Optical point spread functions, for example, are often modelled as Gaussian functions when the sidelobe level is sufficiently low [12].

The results presented in Figure 6 were found to be insensitive to the size of the region selected for autocorrelation analysis. When choosing a region, the main considerations are: (i) the region should contain sufficiently many samples to obtain accurate autocorrelation statistics; (ii) the across track extent should be sufficiently short to ensure a range-invariant impulse response; and (iii) the SAS image should not contain large objects or spatially correlated features.

Although not presented here, it has been verified that intentionally defocusing the SAS during post-processing produces a broadening of the along track intensity autocorrelation function. The corresponding autocorrelation for the complex image remains unchanged. The resolution measurement technique therefore correctly discriminates between focused and defocused imagery. Future work will introduce artificial errors that produce known and quantifiable broadening effects, such as quadratic phase errors, to verify the accuracy of resolution measurement for defocused images.

The method is computationally efficient in that resolution estimation only requires measurement of the autocorrelation at a lag of one sample. When sufficient on-board processing

exists to form SAS images in real-time (e.g. as demonstrated in [11]), the autocorrelation method allows the interesting possibility of estimating resolution “on-the-fly” while adapting the mission plan of an AUV to achieve a desired probability of detection during MCM operations.

REFERENCES

- [1] F. Florin, F. Fohanno, I. Quidu, and J.-P. Malkasse, “Synthetic aperture and 3D imaging for mine hunting sonar” in Proc. Undersea Defence Technology (UDT) Europe, Nice, France, June 23–25, 2004, pp. 1–20.
- [2] M. A. Richards, *Fundamentals of Radar Signal Processing*, chap. 8, McGraw-Hill, 2005.
- [3] D. Billon and F. Fohanno, “Theoretical performance and experimental results for synthetic aperture sonar self-calibration,” in Proc. OCEANS ’98 Conference, Brest, France, September 28–October 1, 1998, vol. 2, pp. 965–970.
- [4] F. Florin, W. Wright, and S. Tomaszewski, “Autonomous system available to enhance US Navy forces MCM capability,” in Proc. 10th International Mine Warfare Technology Symposium, Monterey, CA, May 7–10, 2012.
- [5] Kongsberg Maritime, “HISAS 1030 brochure,” <http://km.kongsberg.com>, retrieved September 7, 2012.
- [6] J. L. Prater, J. L. King, and D. C. Brown, “Determination of image resolution from SAS image statistics,” in Proc. MTS/IEEE OCEANS Conference, Washington, DC, USA, 2015.
- [7] M. Born and E. Wolf, *Principles of Optics*, chap. 7, Cambridge University Press, 7th edition, 1999.
- [8] I. G. Cumming and F. H. Wong, *Digital Processing of Synthetic Aperture Radar Data*, chap. 4, Artech House, 2005.
- [9] J. W. Goodman, *Statistical Optics*, chap. 3, Wiley-Interscience, 1985.
- [10] M. Pinto, “Interferometric synthetic aperture sonar design optimized for high area coverage shallow water bathymetric survey,” in Proc. Underwater Acoustic Measurements, Kos, Greece, June 20–24, 2011.
- [11] J. Dillon, “Real-time interferometric SAS processing with ultra-low power consumption,” in Proc. OCEANS 2018 Conference, Charleston, SC, USA, October 22–25, 2018.
- [12] M. Raffel, C. E. Willert, S. T. Wereley, and J. Kompenhans, *Particle Image Velocimetry: A Practical Guide*, Springer, 2nd edition, 2007.